Measuring representative volume elements from high-resolution grain-scale strain fields

R.B. Vieira[1,*], J. Lambros[2]

[1]Mechanical Engineering, Pontifícia Universidade Católica do Rio de Janeiro, Rio de Janeiro, Brazil
[2]Aerospace Engineering, University of Illinois at Urbana-Champaign, Urbana, 61801, IL.
* corresponding author: renatovieira@puc-rio.br

Abstract

Most crystalline materials present a highly heterogeneous response at the microscale, which can be affected by both internal factors (such as microstructural parameters) and external factors (such as loading). Relating microscale inhomogeneities to the macroscale response of a material requires the use of homogenization techniques, usually based on the concept of a Representative Volume Element (RVE) – the smallest volume of material that represents the global average response. In this work we present a new and robust experimental method of measuring the size of a strain-based RVE from high-resolution grain-scale strain fields obtained using Digital Image Correlation (DIC). The proposed method is based on the statistical (stereological) nature of the RVE, which has been widely adopted in numerical studies, and involves dividing a strain field into randomly selected regions of varying sizes and statistically analyzing the distributions of average strains within them. To validate the new method, we generate a large number of synthetic strain fields from a fractional Gaussian noise algorithm. The proposed stereological method is shown to be capable of producing reliable RVE measurements from a very large range of possible microscale strain fields while at the same time being robust in that it can produce RVE measurement results even in cases where other existing methods may be unable to do so. The proposed method has a low field-of-view requirement, only needing a field-of-view about 1.2 times as large as the RVE to produce reliable measurements. In addition, the stereological method offers significant flexibility since its statistical nature allows for control over how strict the RVE measurement should be in each case.

Key words: Representative volume elements, Digital image correlation, Plastic strains, Statistical volume element

Strain

Introduction

It is well established that strain heterogeneities at microscale are closely related to material response at the macroscale in crystalline metals [1, 2], with many studies exploring formation and development of strain heterogeneities in polycrystals subjected to various loading conditions. For example, under plastic deformation Sachtleber et al. [3] used a photogrammetry-based digital image correlation (DIC) method to measure surface strains in aluminum polycrystal samples with columnar coarse grains and identified triple-points as preferential for strain localization. In fatigue, Abuzaid et al. [4] used a high-resolution DIC technique to measure strain inhomogeneities at the grain scale and their correlations to micro-crack nucleation in a nickel superalloy. During creep, Chen et al. [5] used an in situ neutron diffraction technique to measure the axial internal strains for different family of grains in a pre-strained austenitic stainless steel loaded at varying temperatures, reporting no change in the axial internal strains during creep at 550°C.

On the numerical side, many of the studies that investigate heterogeneous strain development at the microscale have as their goal the validation of micromechanical and/or crystal plasticity models, e.g., [6], where microscale behavior is simulated and then homogenized in some fashion to predict macroscopic response. Such homogenization methods must be performed within a volume of material that has been described by Hill [7] as being able to reproduce the average value of some property of the bulk material, forming the basis of the concept of a Representative Volume Element (RVE). Many authors have recognized the existence of multiple RVEs, coining the terms microstructural volume element or property volume element, to respectively describe an RVE capable of reproducing macroscale average microstructural properties (e.g., grain size, twin density, misorientation distribution) or mechanical properties (e.g., moduli, yield strength, strain distribution) [8]. Bagri et al. [9] recognized the existence of different types of RVE, highlighting

the inherently statistical nature of the RVE. Earlier, Swaminathan et al. [10, 11], described the RVE as the smallest microstructural domain for which statistical distributions of morphological parameters, or material properties, converge to those for the entire microstructure, introducing the term “statistically equivalent RVE”. With this understanding, the RVE is required to reflect not only the average macroscale property, but also its statistical distribution. Experimentally, these distributions can be thought of as the natural variations on the response from a series of samples cut from the same bulk material, i.e., material-induced scatter. These variations are inherently present in polycrystals because of the random nature of the process of crystal formation and can vary in severity depending on the property of interest, for example, material-induced scatter of fatigue life will be much larger than scatter in elastic modulus, and on material texture.

With the RVE playing such a central role in homogenization methods, it is only natural that there has been much study concerning the estimation of RVE sizes for different materials and properties. Bargmann et al. [12] made an extensive review of numerical methods for RVE estimation, including many statistical approaches for a range of different materials. Githens et al. [13] characterized microscale deformation mechanisms of a high strength magnesium rare-earth alloy using crystal plasticity simulations and homogenization. Motaman et al. [14] conducted a study on anisotropic polycrystal plasticity on additively manufactured metallic materials by modeling the microstructure through homogenization techniques. Ranganathan and Ostoja-Starzewski [15] used stochastic boundary value problems to estimate the size of an RVE in random polycrystals. Salahouelhadj and Haddadi [16] estimated RVE sizes for copper polycrystals using homogenization techniques and finite element simulations. Among many other such studies, of special relevance to the present effort is the recent stereological approach of Critchfield and Johnson [17] where they select multiple random samples from within a numerically simulated

domain in order to statistically estimate the RVE size. On the experimental side, a few studies have developed methods of measuring RVE size, with one of the earliest being by Liu [18] who introduced the idea of using full-field strain measurements to determine the size of a strain-based RVE. Efstathiou et al. [19] present another method of experimentally determining the size of a strain-based RVE, using the standard deviation of the average strains in different regions of the strain field as a measure of the homogenization of strains. More recently, Ravindran et al. [20] proposed a method of experimentally measuring a strain-based RVE based on the average strain of an increasing square portion of the microstructure. A few other studies have made attempts at measuring the RVE size experimentally [21, 22], with most of them making use of full-field strain measurement techniques to estimate the size of the strain-based RVE.

The objective of the present work is to develop a robust stereological methodology of measuring the size of an RVE based on experimental grain-level strain fields which will provide not only an average single-valued RVE size, but a statistical variation based on specific microstructural distributions of strain. We will draw from the advantages of existing techniques that have been proposed for measuring average RVE size combining them with approaches for the numerical estimation of RVEs that are statistically based. The proposed method of experimentally measuring strain-based RVEs will thus account for its statistical nature.

High Resolution DIC Grain Scale Strain Fields

The experimental data from which the RVE size will ultimately be obtained consist of digital image correlation (DIC) measurements of residual plastic strains at the grain scale of a polycrystalline material. Through the correlation of undeformed and deformed images of a surface covered by a random speckle pattern, DIC provides full-field displacement and strain measurements on the surface [23]. These measurements have no inherent length scale, which

means that as long as the correlated images have sufficiently high resolution and appropriately scaled speckle pattern, DIC can be used to measure strains across multiple length. Depending on optical magnification and material grain size, the high-resolution DIC (HiDIC) technique [24] is capable of discerning non-uniformities in the strain field at the microstructural level through the use of images taken under an optical microscope. One disadvantage of this approach is the reduced field-of-view resulting from the high magnification needed to obtain grain-level information. A larger field-of-view can be achieved by taking a series of images in a grid covering a larger region of interest and stitching the images together [24]. If this image-stitching approach is followed, measurements are then limited to capturing residual strains left in the material after unloading since the sample would have to be removed from the loading fixture in order to be placed under an optical microscope (i.e., an ex situ measurement approach).

The experimental results shown here were obtained using such an ex situ approach under an optical microscope with ~0.1 μm/pixel resolution images after loading the sample under creep conditions. Creep loading was selected in order to allow for a convenient way to introduce plastic strains amenable to an ex situ measurement methodology. A grid of 6 by 6 images was taken of the sample surface (with an overlap of 50%), using a 2000 by 2000 pixel detector, to cover a region of interest of about 400 by 400 μm. These images were then stitched together using the built-in stitching function in Fiji ImageJ [25], and the resulting sets of stitched images were used for correlation with a subset size of 61 pixels (~6 μm) and a step size of 10 pixels (~1 μm). More details of the experimental method are given in [26, 27]. Here we will restrict ourselves to presenting only a sampling of the experimental results and rather we will concentrate on describing the methodology for stereological extraction of RVE size. Fig. 1 shows examples of the resulting axial strain field obtained measured using HiDIC for two austenitic stainless steel 709 samples.

Sample 1 (Fig. 1a) was loaded to 80 MPa for 1 hour at 800°C (~25% below yield stress at 800°C), while sample 2 (Fig. 1b) was loaded to 215 MPa for 1 hour at 300°C (~25% below yield stress at 300°C). The strain fields have been overlaid with the grain boundaries obtained through an electron backscatter diffraction (EBSD) scan of the same area of the samples before loading. The resulting strain fields for both samples show very pronounced inhomogeneity, and although both instances correspond to conditions of 1 hour creep at a stress of 25% below their corresponding yield point, at least visually, appear very different from one another when plotted on the same contour scale. The next section will go over the use of two existing experimental methods of measuring the strain-based RVE sizes for these samples and discuss the applications of each one.

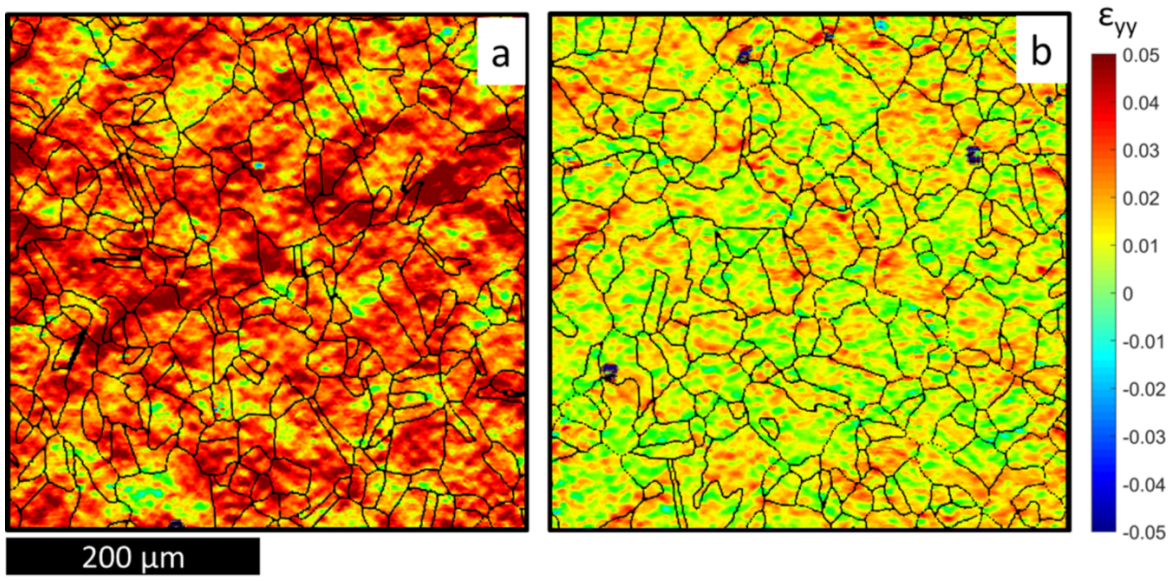

Fig. 1. Residual strains along the vertical loading direction (ε_{yy}) obtained for two stainless steel samples loaded to 25% below yield strength for 1 hour at (a) 800°C and (b) 300°C, overlaid with grain boundaries (black lines) obtained from EBSD.

Application of Two Experimental RVE Measurement Methods

Standard deviation method

What we will refer to as the "standard deviation method" follows closely the method developed by Efstathiou et al. [19]: dividing the strain field into a grid of boxes of the same size and observing the variation of the standard deviation of the box averages vs. the size of the boxes. First, the field is divided into a grid of boxes of the same size, starting from the top-left corner the strain field is divided into a grid, with the portion to the right and bottom where another box wouldn't fit being left out of the calculations. Then the average strain of each box is calculated, and finally, the standard deviation of these averages is computed. This is repeated for each box size, varying from the size of the entire field of view to a 1x1 pixel "box". The RVE size is then determined by fitting a line to the trailing points and assuming a large deviation from linearity to be a result of a box size considerably smaller than the RVE. Fig. 2a shows the plot for the standard deviation of box average strains vs. the box size for sample 1. In this case, a large deviation from linearity is observed for a box size around 100 μm, and this value is taken as the RVE size for sample 1. The inset in Fig. 2a shows the strain field with the obtained RVE size box drawn in the upper left corner. Note that from this point forward, the RVE sizes will be reported as a single length value, which should be understood as the side of a 2D square box, i.e., in this case the RVE shown is 100 μm by 100 μm box on the surface. In fact, since only surface measurements are used in this computation, a limitation of 2D DIC, perhaps it is more appropriate to call this region a Representative Surface Element (RSE), but as is common in the literature we will assume that the size of the RVE into the third dimension mimics its size on the surface (i.e., the RVE is assumed to be a 100 μm by 100 μm by 100 μm box).

A limitation of this method is already apparent by looking at the box sizes from 200 to 400 μm in the plot of Fig. 2a. Since these boxes are larger than half the size of the entire field, only a single box can fit inside of it, hence the standard deviation of the averages for all box sizes from 200 to 400 μm falls to 0. Ultimately this means that this method is only able to measure an RVE that is considerably smaller than the field of view. In other words, this method requires strain measurements spanning relatively large areas of the surface that far exceed the (expected) RVE size. This limitation is illustrated in Fig. 2b which shows the equivalent plot obtained for sample 2, where it is clear that the standard deviation method is not well suited to measuring the RVE size for this sample, since the trailing points would result in a very poorly fitted line. This happens because sample 2 has an RVE size close to half the field of view (as will be seen below).

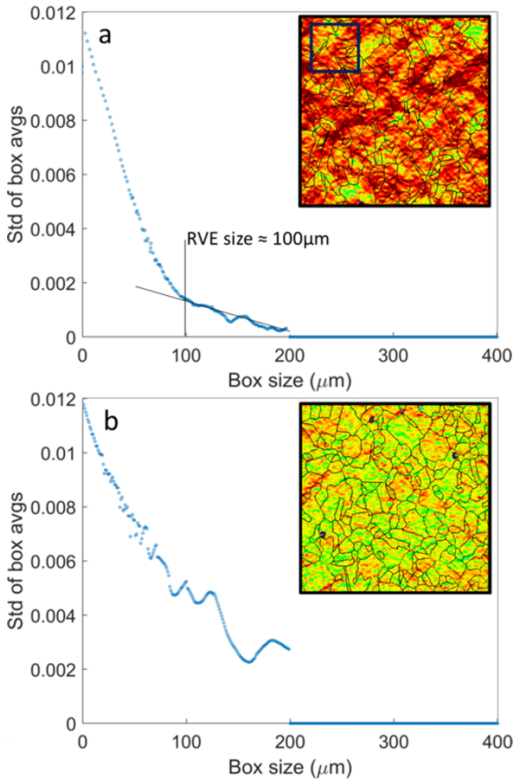

Fig. 2. Standard deviation method plots for (a) sample 1 and (b) sample 2; insets show the respective strain fields with the obtained RVE sizes drawn (this method is not suited for measuring the RVE of sample 2).

Centered box growth method

The second method explored here follows Ravindran et al. [20], and will be referred to as the "centered box growth method". As the name suggests, the method uses a single box grown from the center point of the strain field and plots the average strain inside the box vs. box size. The RVE size is then determined by evaluating convergence of the average strain within some margin of error. Although this range can be varied, following [20] a ±5% margin is used here to check for convergence of the average strain to the global average of the strain field. Note that in the experiments the average macroscale axial strain is measured from lower-resolution in-situ DIC. The point beyond which the box average strains converges to within 5% of the global average is taken as the RVE size. Fig. 3 shows how this method can be applied to (a) sample 1 and (b) sample 2, with insets showing the respective strain fields overlaid by the obtained RVE sizes.

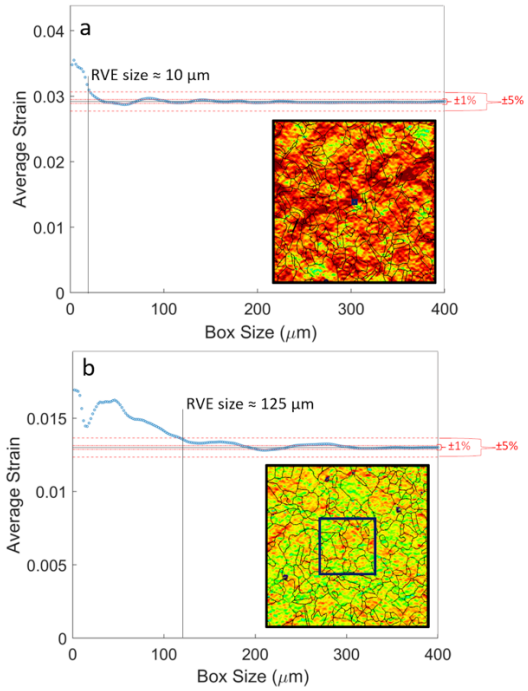

Fig. 3. Centered box growth method plots for (a) sample 1 and (b) sample 2; insets show the respective strain fields with the obtained RVE sizes drawn (horizontal lines show the global average strain far-field measured from in-situ DIC, and ±1% and ±5% bands from the average).

An advantage of this method is that it will produce an estimate of the RVE size as long as the field of view is slightly larger than the size of an RVE (the estimated field of view requirement is about 1.2 times the RVE size). Because of this, the centered box growth method was able to produce a result for sample 2 (Fig. 3b) even though the standard deviation method was unable to do so. This means that the centered box growth method can be applied with a field of view about half the size of that required by the standard deviation method. However, using a single box grown from the center of the field of view also makes the method highly dependent on the starting location and the distribution of strains directly surrounding this starting location – issues which ultimately can result in unreliable RVE size estimates in some cases. Fig. 3a shows the resulting RVE size obtained for sample 1 using the centered box growth to be 10 μm, which appears unrealistic (recall that the standard deviation method obtained an RVE size of 100 μm for this same case). The distribution of the strains within the field of view, as well as the fact that the center pixels of the strain field for sample 1 happen to be close to the average value, cause this erroneous measurement of a 10 μm RVE, because the average box strains converged to the global average strain (as measured from in-situ DIC) at a very small box size. Statistically speaking, finding an RVE size of 10 μm for this sample is an anomaly that happens because of the random nature of microstructural distributions, especially given the fact that the average grain size in this material is about 25 μm. In fact, these two samples were chosen to illustrate that although each of these methods have specific advantages, they do not always converge to a reasonable measurement of a single-valued RVE size. In the next section we propose a new method that takes into account these statistical variations by considering the RVE as an inherently statistical entity, i.e., a probability distribution rather than a fixed value.

Stereological RVE Measurement Method

The method proposed here will be able to measure the RVE from fields of the order of the RVE size and also account for the dependence on the location and strain distributions. As discussed earlier, previous authors [10, 11] have recognized the statistical characteristic of the RVE, although less effort has been made to incorporate this feature in experimental studies. In order to develop a new method that takes the statistical aspect of the RVE into account, a large quantity of strain data for which the RVE size is controllable is necessary. Such a large number of separate datasets is extremely difficult, if not impossible, to obtain experimentally. Therefore, here we will first generate highly controllable synthetic "strain fields" that are qualitatively and quantitatively similar to those obtained by HiDIC, but for which we can control geometric features so as to control the resulting RVE size. The proposed method will be developed and verified based on these synthetic strain fields, and will then be validated on experimentally measured data.

Controllable synthetic "strain" fields

The procedure used here to generate controllable synthetic strain fields consists of a simplified version of the fractional Gaussian noise introduced by Mandelbrot and van Ness [28]. Different frequencies of Gaussian noise are generated by taking n by n matrices of random values obtained from the standard normal distribution (using the randn Matlab function which uses a Mersenne twister generator [29] to produce random values from the standard normal distribution) and interpolating them through a cubic spline with not-a-knot end conditions to span the size of the final image (the interpolation was done using the Matlab function interp2 with the 'method' parameter set to 'spline'). Fig. 4 shows how single-frequency Gaussian noise can be obtained by a spline interpolation of a 31 by 31 matrix of random values, from the standard normal distribution, to a 500 by 500 pixel image. Then, a synthetic strain field is obtained by adding different frequency

Gaussian noises together, multiplied by a weight factor inversely proportional to the frequency (i.e., higher frequencies have lower weights). Fig. 5 shows schematically how Gaussian noise obtained from varying squared matrix sizes of 500, 250, 125, 62 and 31 pixels can be multiplied by increasing weights of 1x, 2x, 3x, 4x and 5x respectively, and added together to obtain a synthetic strain field.

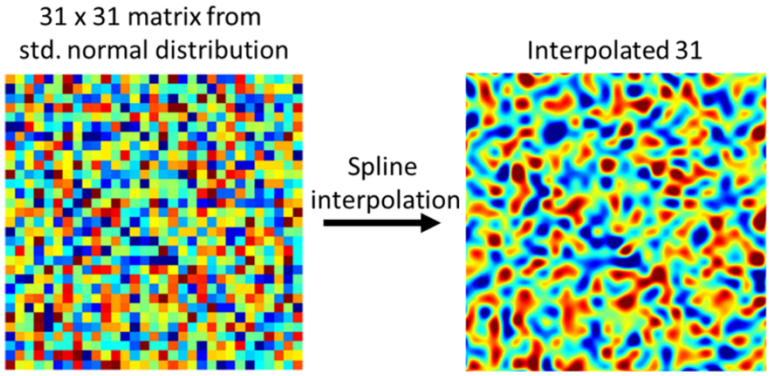

Fig. 4. Obtaining one frequency Gaussian noise by spline-interpolating a 31 by 31 matrix of random values, from the standard normal distribution, to a 500 by 500 pixel image.

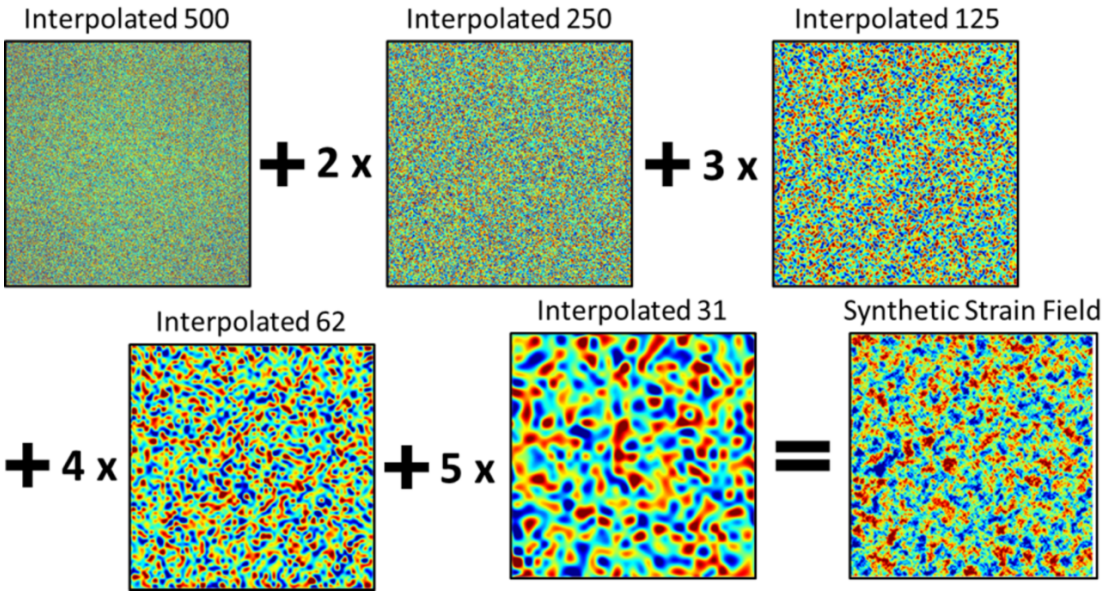

Fig. 5. Different Gaussian noise frequencies are added together, multiplied by inversely proportional weights, to obtain a synthetic strain field.

The geometric scale (which is closely related to the RVE size) of the final synthetic strain field can be controlled by choosing what frequencies of Gaussian noise are added together. A scale factor was introduced as a single parameter that controls the geometric scale of the synthetic strain fields, as a way to summarize the noise frequencies from which it was composed. The procedure to obtain a synthetic strain field of a given scale factor (SF) can be more rigorously described by equation 1.

$$SyntheticField(SF) = \sum_{n=SF+1}^{15} (16 - n) \cdot Int(f_n) \quad (1)$$

, where f_n are the components of f=[2,3,4,5,6,7,8,9,10,15,31,62,125,250,500] and Int(f_n) is the 500 x 500 matrix interpolated from the f_n x f_n matrix of random values from the standard normal distribution.

For example, if a scale factor of 14 was used, the synthetic strain field generated would consist of only the 500 by 500 interpolated matrix multiplied by a weight of 1, while for a scale factor of 8, interpolated matrices of sizes 500, 250, 125, 62, 31, 15 and 10 would be interpolated and added together with the corresponding weights of 1, 2, 3, 4, 5, 6 and 7.

The final step in obtaining synthetic fields comparable to the strain fields shown in Fig. 1 is to normalize their values (so that average strain values of the synthetic fields have values of the order of the real experimental fields with similar distributions) and re-plot the synthetic strain fields with the same contour limits. Equation 2 shows the normalization and rescaling procedure to obtain a synthetic “strain” field (similar to the real experimental strain fields) from the synthetic fields obtained in equation 1.

$$SyntheticStrainField(SF) = 0.02 \cdot \frac{SyntheticField(SF)}{\overline{SyntheticField(SF)}} \quad (2)$$

,where 0.02 is the average strain from all the real experimental data and $\overline{SyntheticField(SF)}$ is the average value of the synthetic field obtained from Equation 1.

Representative synthetic fields for scale factors 6, 8, and 10 are shown in Fig. 6, illustrating how the scale factor can be used to control the geometric scale of these fields, which is directly related to the size of the RVE. Fig. 6 also shows histograms of the "strain" values for each of the three synthetic "strain" fields (d, e and f), as well as the histogram of the strain distribution obtained for sample 2, for comparison (Fig. 6g). All these distributions look very similar to one another, which is what we need, since we would want the only real difference between them to be the geographical distribution of the "strains" within the field. Note that we do not have an a priori closed form mathematical result of what this RVE size would be, although it is clear from the figure that the RVE size varies with scale factor. In addition, these images resemble different variations of strain field similar to those seen in Fig. 1, although the numerical values do not represent actual strains since there is no guarantee that these "strain" fields are compatible. These synthetic strain fields should be treated as mathematical entities capable of providing images with controllable length scales (and resulting RVE sizes), and thus should not be used to generate any mechanical evaluation of real strain or material behavior. However, their usefulness lies in that very large numbers of unique "strain" fields, similar to the ones obtained from real experimental data, can be generate and used to develop and verify the proposed RVE measurement method.

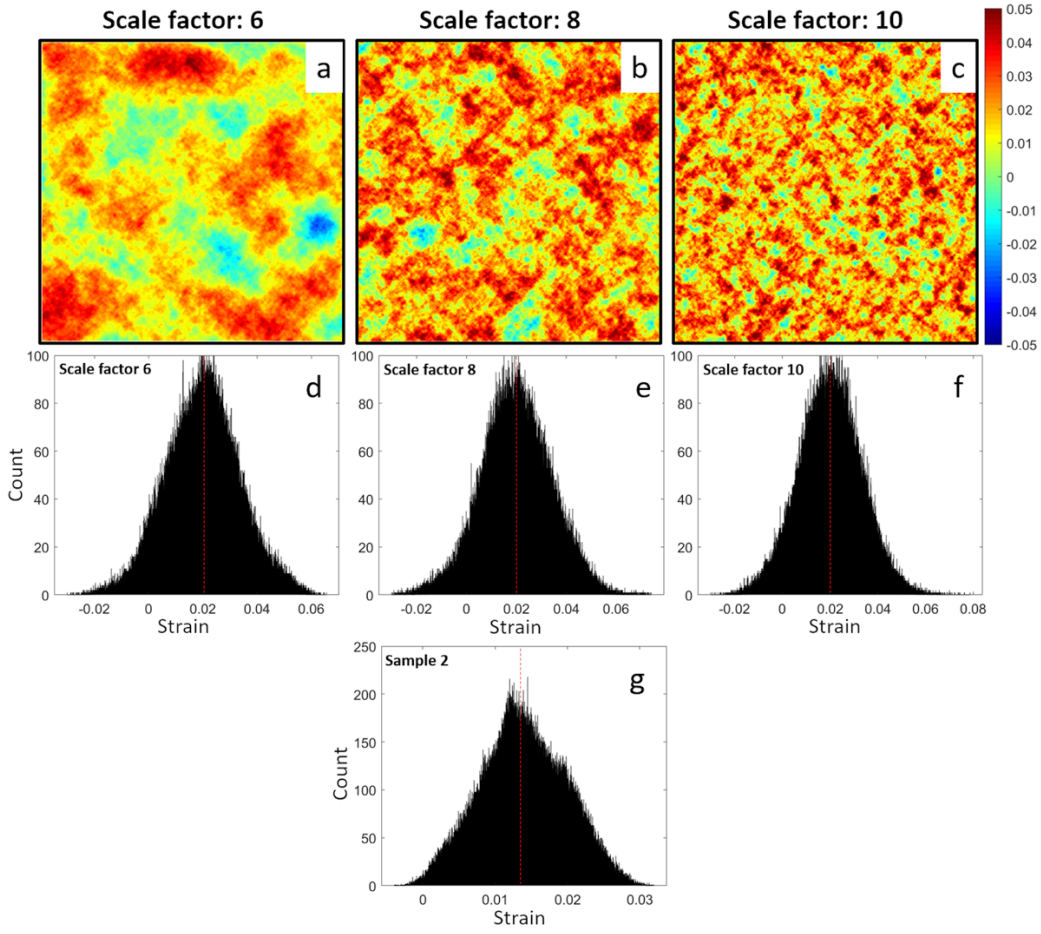

Fig. 6. Representative synthetic strain fields and histograms of the strains found for scale factors (a) 6; (b) 8; (c) 10. For comparison, (g) shows the histogram of strains from sample 2.

Stereological approach

The proposed stereological method consists of taking a large number of randomly distributed boxes from within the field of view and plotting a histogram of the average box strains for each box size. Then, the RVE size can be determined, similarly to the centered box growth method, through the use of a margin around the global average strain (as measured from lower-resolution in-situ DIC), also allowing for a choice on how strict the measurement should be, by choosing what percentage of the boxes should fall within the margin. Fig. 7a shows a synthetic strain field with a scale factor of 8, superimposed by a few randomly distributed boxes of size 191

pixels. Fig. 7b shows the histograms obtained by taking 10,000 randomly distributed boxes of sizes 10, 191 and 350 pixels. From Fig. 7b it is possible to see that for a box size of 10 pixels, few (less than 10%) of the boxes fall within the ±5% margin from the global average strain. With a box size of 191 pixels, 80% of the boxes fall within the ±5% margin, while for a box of 350 pixels 80% of the boxes fall within a ±1% margin of the global average strain. These two ranges can be understood as a confidence level and a margin of error: 80% of the time a box of size 191 pixels will be a strain-based RVE (i.e., will reflect the global average strain), considering a margin of error of ±5% on the strains, or 80% of the time a box of size 350 pixels will be a strain-based RVE, considering a margin of error of ±1% on the strains. Using this inherently statistical approach, we can see how the statistically anomalous result obtained from the centered box growth method for sample 1 (Fig. 3a) could be possible (it would be one of the few boxes in the 10-pixel histogram that fall within the ±5% margin in Fig. 7b).

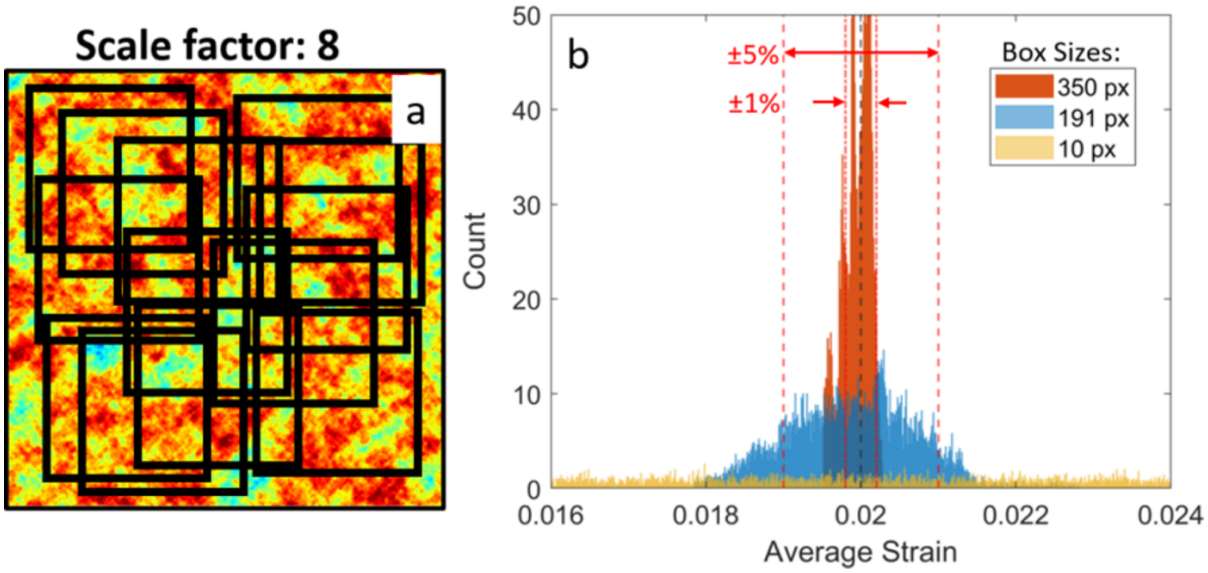

Fig. 7. (a) Synthetic strain field with scale factor 8 superimposed by randomly distributed boxes of size 191 pixels; (b) Histograms of average strains for a box sizes of 10 pixels, 191 pixels, when 80% of the boxes fall within a ±5% margin from the global average strain, and 350 pixels, where 80% of the boxes fall within a ±1% margin of the global average

Number of boxes selection

Apart from the margin of error and the confidence level (or threshold level), that should be selected according to the noise level of experimental data and the desired strictness of the measurement (see discussion of Fig. 11), one other parameter that that can be varied when applying the stereological method is the number of randomly selected boxes that are taken from within the strain field. In the example of Fig. 7, 10,000 boxes were selected, which allowed the threshold value of 80% to be evaluated as 8,000 out of the 10,000 boxes. This lowers the probability that for a given strain field, by chance, the selected boxes end up converging to the global average at a much smaller box size, resulting in an erroneous RVE size measurement.

It is important to note that by taking 10,000 randomly selected boxes from the strain field, overlap of sampling boxes is to be expected for larger box sizes. This might introduce some systematic error, but it also guarantees that the entire strain field will be covered. In contrast, for example the sampling method used in the standard deviation method, where dividing the field into a regular non-overlapping grid, is bound to leave some strain field data unaccounted for when the box size does not exactly tessellate the region of interest. The requirement that the entire strain field data be represented for all box sizes considered is of course dependent on the strain field develop and thus the number of boxes used is not a universally fixed quantity, but rather is a parameter that could be adjusted depending on the relative scale of image, microstructure and resulting strain field.

For the fields considered here, a study on the influence of the number of boxes on the resulting RVE size was conducted and is shown in Fig. 8. The RVE size of synthetic “strain” fields of scale factors of 0, 3, 6, 8 and 10 was measured using the stereological method with a margin of ±5%, a threshold of 80% and different number of boxes (100, 1,000, 5,000, 10,000 and 20,000).

For each point in Fig. 8, 1,000 different synthetic "strain" fields were generated, and the median RVE size measured was plotted. The error bars show the maximum and minimum RVE sizes measured out of those 1,000 runs.

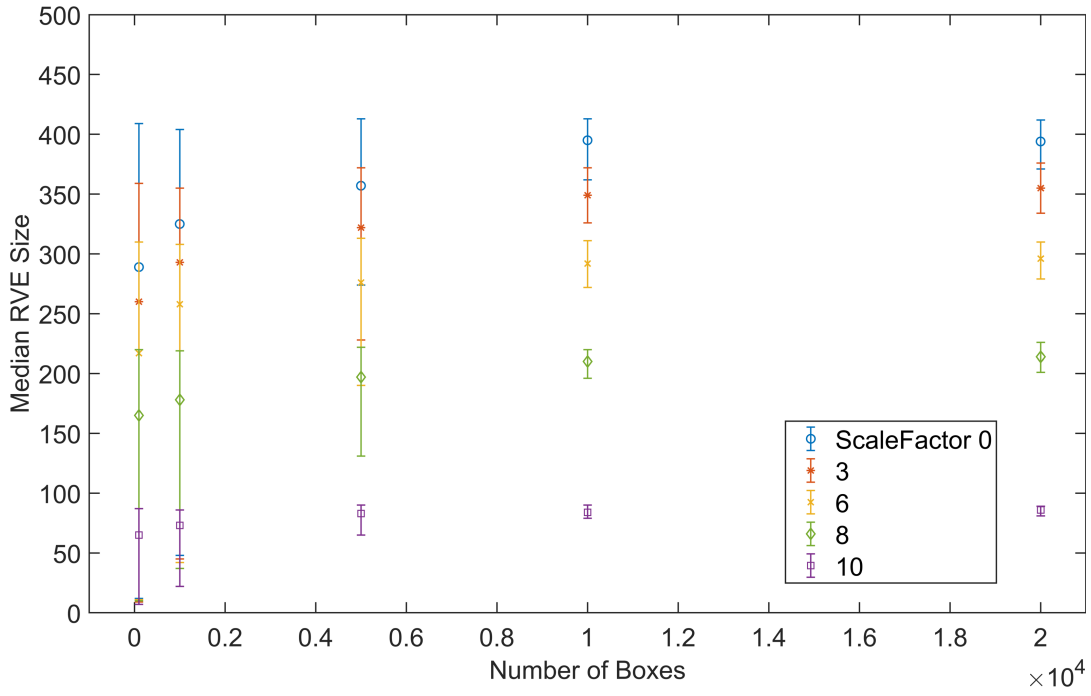

Fig. 8. Plot of median RVE size measured vs Number of boxes used. Each point was obtained from applying the stereological method to 1,000 different synthetic "strain" fields and calculating the median RVE size measured. Error bars show the maximum and minimum RVE sizes obtained.

This result shows how the number of boxes can affect the results for RVE size. With lower number of boxes, there is a higher probability that for a single strain field the method gives an erroneous result, which happens when, by chance, 80% of the randomly selected boxes fall within the margin from the global average strain. This is made clear from the lower values for the median and minimum RVE sizes measured with fewer boxes (mainly 100 and 1,000 boxes in Fig. 8). Accordingly, with higher number of randomly selected boxes, the chance that the method gives an

erroneous result becomes much lower, which can be seen from the tighter margin between the minimum and maximum RVE size results.

The main observation from Fig. 8 that highlights the statistical nature of the RVE comes from the fact that for all number of randomly selected boxes the maximum RVE size measured was fairly constant. What that shows is that even with a very low number of boxes, from 1,000 runs of the method, at least one of them was able to produce a realistic result for the RVE size. In fact, the maximum measured RVE size should be considered the "real" RVE size for each scale factor, with the median and minimum giving an idea of how likely the method is to produce a good result from a single run. From these results, a number of boxes of 10,000 was selected as a good number for strain fields within the studied range of RVE sizes, and is therefore the number of boxes used in all further examples. Nonetheless, it is also clear that for some situations fewer boxes could be used, reducing the overlapping that is bound to happen for larger number of boxes.

Statistical equivalence between stereological method and box growth method

In order to validate the proposed stereological method, it must be shown that it can predict similar RVE sizes as the existing methods, as well as their statistical variation. Although with the proposed method we can generate histograms from one dataset by subdividing it randomly in the desired number of boxes, in the centered box growth method only one RVE measurement can be made per dataset. To this end, the centered box growth method was applied to 10,000 *different* synthetic strain fields with scale factors from 0 to 10 (using a ±5% margin from global average strains to judge convergence as in [20]), with the results obtained for fields of scale factor 8 being plotted in the histogram shown in Fig. 9a as an example. For this case, vertical lines in Fig. 9a indicate the values of the median, average, and 80% threshold level, the latter defined as the location (232 pixels in this case) where for 8,000 of the 10,000 synthetic strain fields the centered

box growth method predicts an RVE size of at most that pixel value (i.e., for 80% of cases 232 pixels is an RVE or lower). With this result (obtained through the use of 10,000 *different* synthetic strain fields), it is possible to compare the statistical predictions from the centered box growth method to the proposed stereological method. Fig. 9b shows a plot comparing the results obtained from the 80% threshold of both the centered box growth (with 10,000 *different* synthetic strain fields being analyzed for each point) and the stereological method (with 10,000 boxes taken from a *single* synthetic strain field for each point) for scale factors from 0 to 10. The *single* synthetic field to which the stereological method was applied was selected at random from the pool of 10,000 *different* synthetic strain fields to which the centered box growth method was applied.

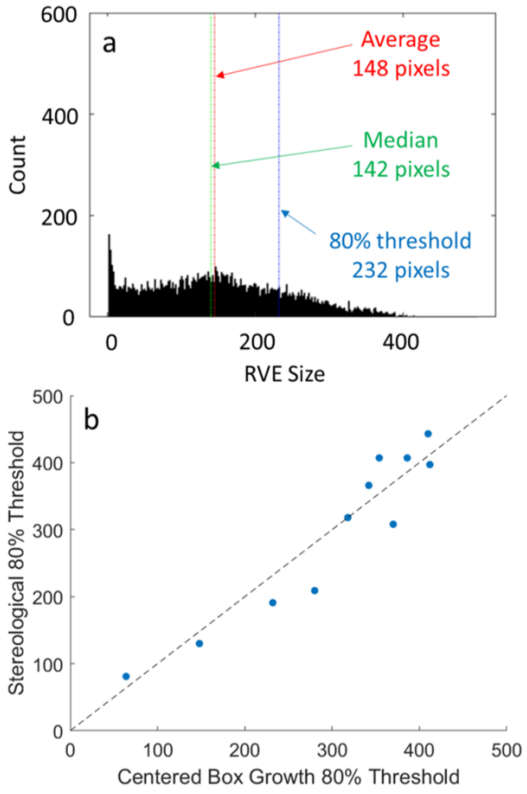

Fig. 9. (a) Histogram of the results obtained from the centered box growth method (±5% margin on strains) for 10,000 *different* synthetic strain fields of scale factor 8; b) Plot of the RVE sizes measured by the stereological method vs. the centered box growth method, both using the 80% threshold and a ±5% margin on strains.

The data points of Fig. 9b show that the stereological method produces statistically equivalent results to the centered box growth method, while requiring far less data to do so (a single image vs. 10,000 different images). Thus, one advantage of the stereological method is that by taking into account the statistical variance of the RVE size, the method is able to consistently predict a wide range of strain-based RVE sizes from a single strain field regardless of the particular random distribution of strains within the field of view of each sample.

Application to experimental results

Here we will apply the stereological method to the same experimental data, namely those of Fig. 1a, where the standard deviation method produced reasonable results but the centered box growth method did not, and those of Fig. 1b where the opposite occurred. Fig. 10 shows the histograms obtained for (a) sample 1 and (b) sample 2, using the 80% threshold and a ±5% margin on strains (80% of the randomly selected boxes fall within the ±5% margin from global average strains, as measured from lower-resolution in-situ DIC). The insets show the respective strain fields overlaid by a box of size equal to the strain-based RVE measured using the stereological approach, namely 94 μm and 152 μm respectively.

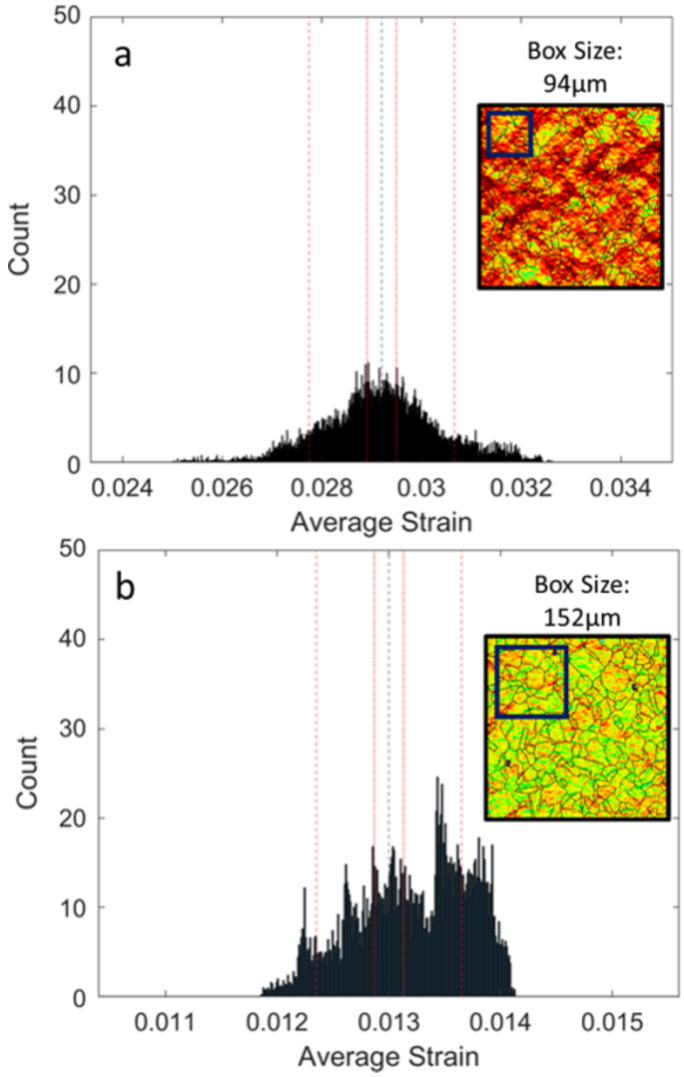

Fig. 10. Stereological method plots for (a) sample 1 and (b) sample 2; insets show the respective strain fields with the obtained RVE sizes drawn (the RVE size was taken at the 80% threshold considering a ±5% margin on strains).

Table 1 shows the strain-based RVE sizes measured for each sample from each of the three discussed experimental methods. Note that the stereological method was successful in measuring a reasonable (i.e., comparable to the other method(s)) RVE size for both samples, while the standard deviation method failed entirely to produce an estimate for sample 1 and the centered box growth method resulted in an unrealistic prediction for sample 2. These results show that the stereological method is a robust way of experimentally measuring the size of the strain-based RVE.

The method is also more flexible since it is capable of being adjusted to match the desired strictness level of the measurement, by for example choosing a different threshold value, as seen in the 90% and 99% columns of the stereological method in Table 1, or a tighter margin for the strains.

Table 1. Strain-based RVE sizes measured for two samples using each of the three discussed methods.

	Standard Deviation method	Centered Box Growth method (±5% margin from global avg. strain)	Stereological method (±5% margin from global avg. strain)		
			80% Threshold	90% Threshold	99% Threshold
Sample 1	100 µm	10 µm	94 µm	112 µm	149 µm
Sample 2	-	125 µm	152 µm	168 µm	218 µm

For the purposes of comparing the stereological method with the two prior methods which offer deterministic single-valued RVE results, all the strain-based RVE sizes quoted above in Table 1 were taken using fixed thresholds of 80%, 90% or 99% and a ±5% margin from the global average strain. However, the stereological method can in fact also be used to generate a probability distribution for the size of the strain-based RVE. If instead of choosing a priori a threshold and interrogating the strain field to determine what box size converges to the global average (within a chosen margin which, for example, can be based on experimental noise levels), we do the opposite and calculate what percentage of the randomly selected boxes fall within the chosen margin, then a probability distribution can be plotted. Fig. 11 shows the probability that the box average strain falls within a ±5% or a ±1% margin from the global average strain for each box size in sample 2 (Fig. 1b). The 80%, 90% and 99% threshold lines are shown, for reference, but this plot makes it clear how the stereological method could be used with different combinations of threshold and margin to produce more (or less) strict strain-based RVE size measurements. Furthermore, it is

clear from Fig. 11 that the variation of the RVE size probability with the ±1% margin on strains appears noisier than that with ±5% margin, indicating that the margin should be selected according to the expected noise level of the experimental results (i.e., 1% is too tight of a margin for the present HiDIC results).

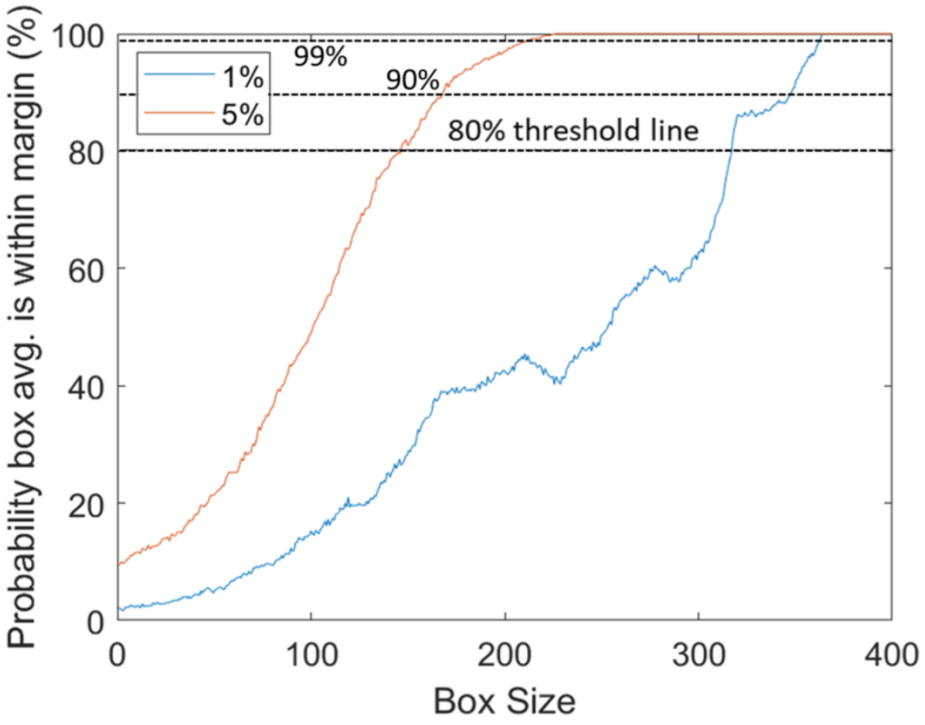

Fig. 11. Probability that the average strain from a random box falls within the global average strain vs. box size, for ±5% and ±1% margins. The 80%, 90% and 99% threshold lines are shown, for reference.

For simulation purposes, where the RVE is to be used as a simulation box to save on computational costs, a single-valued RVE size would be necessary, and thus a specific value for the threshold must be selected. This selection of threshold value should be done by taking into account the variability of the microstructure in question and the desired strictness level of the measurement (i.e., more uniform microstructures could use higher thresholds while more heterogeneous microstructures would require lower thresholds). Not only that, but the selection of

threshold could also take into account possible boundary condition effects, which will always be present in any simulation. The application of RVE sizes experimentally measured using the proposed stereological method is beyond the scope of the present work, and shall be the focus of future studies.

Conclusions

The review of two experimental methods from the literature (namely the standard deviation and the centered box growth methods) made it clear that there is still a lack of robustness when it comes to experimentally measuring the size of a strain-based RVE. Although based on the sound argument, that the standard deviation of strain averages within boxes should change with box size and that for boxes larger than an RVE this standard deviation should be much lower than for boxes smaller than the RVE, the standard deviation method has one major flaw that affects its robustness. The somewhat arbitrary selection of the linear fit for larger box sizes, which is used to define the size of the RVE, is bound to produce unrealistic results in a few cases (as is clear from Fig. 2). Not only that, but the methodology described by Efstathiou et al. [19] for the linear fit makes it hard to automate the method. On the other hand, the centered box growth method presents a much more well-defined methodology to measure the size of the RVE, making it easier to automate and thus consistently produce results. In order to do that, the method proposed by Ravindran et al. [20] treats the RVE size as a deterministic quantity, instead of observing the inherently statistical nature of the RVE. Through its heuristic analysis, the centered box growth method is bound to produce (by chance) erroneous results in situations where the spatial distribution of strains around the center point of the field of view results in an early convergence to the global average strain.

The objective behind the development of the proposed stereological method was to circumvent the disadvantages of each of these two methods, while using the advantages of both.

The stereological method recognizes the statistical nature of the RVE (similar to the standard deviation method) and uses the ideas of a margin and a threshold (derived from the centered box growth method) to arrive at a robust methodology to measure the size of the strain-based RVE. In fact, it could be argued that the theory behind the stereological and the standard deviation methods is very similar, and that both methods are based on the resulting quasi-normal distribution of average strains that arises from the sampling of boxes from the field of view. The added robustness of the stereological method comes from the methodology used to study this distribution, which was inspired in the centered box growth method, and also gives it the added capability to adapt the measurement to the experimental data in question (as seen in Fig. 11).

Using controllable synthetic strain fields generated through a fractional Gaussian noise algorithm, the proposed stereological method was shown to produce robust RVE size results accompanied by a statistical measure of how often the strain measurements actually converge to the global average. The method was then applied to real DIC experimental measurements and RVE sizes were obtained for two samples loaded at different creep conditions. The following points summarize the findings of this study:

1) The synthetic strain fields obtained from Gaussian noise allow the generation of large quantities of data, similar to the experimental strain fields, with an easily adjustable scale parameter that directly correlates with the resulting RVE size;
2) The proposed stereological method uses the statistical nature of the RVE and builds upon the centered box growth method to produce equivalent RVE measurements along with a statistical measure of how strict the measurement is;
3) The stereological method was shown to produce reliable single-valued RVE size measurements for two very different experimental strain fields obtained using the

HiDIC technique from creep-loaded samples, by using fixed values for the threshold and strain margin;

4) The generalization of the stereological method was showcased by generating a probability distribution for the RVE size of one of the experimental results, with the threshold levels relating to microstructural variability and the strain margin relating to the expected measurement noise levels.

Acknowledgements

The work was carried out in part in the Materials Research Laboratory Central Research Facilities University of Illinois (EBSD measurements), and the Advanced Materials Testing and Evaluation Laboratory University of Illinois (mechanical testing). This research was performed in part using funding received from the Department of Energy Office of Nuclear Energy's Nuclear Energy University Program under grant number DE-NE0008436 (Project number 15-8432) and the National Science Foundation under Grant Nos. CMMI 18-25466 and 20-27082.

References

[1] F. Delaire, J. Raphanel and C. Rey, "Plastic heterogeneities of a copper multicrystal deformed in uniaxial tension: Experimental study and finite element simulations," *Acta Materialia,* vol. 48, pp. 1075-1087, 2000.

[2] D. Raabe, M. Sachtleber, Z. Zhao, F. Roters and S. Zaefferer, "Micromechanical and macromechanical effects in grain scale polycrystal plasticity experimentation and simulation," *Acta Materialia,* vol. 49, pp. 3433-3441, 2001.

[3] M. Sachtleber, Z. Zhao and D. Raabe, "Experimental investigation of plastic grain interaction," *Materials Science and Engineering A,* vol. 336, pp. 81-87, 2002.

[4] W. Abuzaid, H. Sehitoglu and J. Lambros, "Plastic strain localization and fatigue micro-crack formation in Hastelloy X," *Materials Science and Engineering: A,* vol. 561, pp. 507-519, 2013.

[5] B. Chen, J. Hu, Y. Wang, S. Kabra, A. Cocks, D. Smith and P. Flewitt, "Internal strains between grains during creep deformation of an austenitic stainless steel," *Journal of Materials Science,* vol. 50, pp. 5809-5816, 2015.

[6] F. Roters, P. Eisenlohr, L. Hantcherli, D. Tjahjanto, T. Bieler and D. Raabe, "Overview of constitutive laws, kinematics, homogenization and multiscale methods in crystal plasticity finite-element modeling: Theory, experiments, applications," *Acta Materialia,* vol. 58, pp. 1152-1211, 2010.

[7] R. Hill, "Elastic properties of reinforced solids: Some theoretical principles," *Journal of the Mechanics and Physics of Solids,* vol. 11, no. 5, pp. 357-372, 1963.

[8] M. Echlin, A. Mottura, M. Wang, P. Mignone, D. Riley, G. Franks and T. Pollock, "Three-dimensional characterization of the permeability of W–Cu composites using a new “TriBeam” technique," *Acta Materialia,* vol. 64, pp. 307-315, 2014.

[9] A. Bagri, G. Weber, J. Stinville, W. Lenthe, T. Pollock, C. Woodward and S. Ghosh, "Microstructure and Property-Based Statistically Equivalent Representative Volume Elements for Polycrystalline Ni-Based Superalloys Containing Annealing Twins," *Metallurgical and Materials Transactions A,* vol. 49, no. 11, pp. 5727-5744, 2018.

[10] S. Swaminathan, S. Ghosh and N. Pagano, "Statistically Equivalent Representative Volume Elements for Unidirectional Composite Microstructures: Part I - Without Damage," *Journal of Composite Materials,* vol. 40, no. 7, pp. 583-604, 2006.

[11] S. Swaminathan and S. Ghosh, "Statistically Equivalent Representative Volume Elements for Unidirectional Composite Microstructures: Part II - With Interfacial Debonding," *Journal of Composite Materials,* vol. 40, no. 7, pp. 605-621, 2006.

[12] S. Bargmann, B. Klusemann, J. Markmann, J. Schnabel, K. Schneider, C. Soyarslan and J. Wilmers, "Generation of 3D representative volume elements for heterogeneous materials: A review," *Progress in Materials Science,* vol. 96, pp. 322-384, 2018.

[13] A. Githens, S. Ganesan, Z. Chen, J. Allison, V. Sundararaghavan and S. Daly, "Characterizing microscale deformation mechanisms and macroscopic tensile properties of a high strength magnesium rare-earth alloy: A combined experimental and crystal plasticity approach," *Acta Materialia,* vol. 186, pp. 77-94, 2020.

[14] S. Motaman, F. Roters and C. Haase, "Anisotropic polycrystal plasticity due to microstructural heterogeneity: A multi-scale experimental and numerical study on additively manufactured metallic materials," *Acta Materialia,* vol. 185, pp. 340-369, 2020.

[15] S. Ranganathan and M. Ostoja-Starzewski, "Scale-dependent homogenization of inelastic random polycrystals," *Journal of Applied Mechanics,* vol. 75, no. 5, pp. 051008, 2008.

[16] A. Salahouelhadj and H. Haddadi, "Estimation of the size of the RVE for isotropic copper polycrystals by using elastic–plastic finite element homogenisation," *Computational Materials Science,* vol. 48, no. 3, pp. 447-455, 2010.

[17] T. Critchfield and O. Johnson, "Representative and statistical volume elements for grain boundary networks: A stereological approach," *Acta Materialia,* vol. 188, pp. 166-180, 2020.

[18] C. Liu, "On the Minimum Size of Representative Volume Element: An Experimental Investigation," *Experimental Mechanics,* vol. 45, no. 3, pp. 238-243, 2005.

[19] C. Efstathiou, H. Sehitoglu and J. Lambros, "Multiscale strain measurements of plastically deforming polycrystalline titanium: Role of deformation heterogeneities," *International Journal of Plasticity,* vol. 26, no. 1, pp. 93-106, 2010.

[20] S. Ravindran, B. Koohbor and A. Kidane, "Experimental characterization of meso-scale deformation mechanisms and the RVE size in plastically deformed carbon steel," *Strain,* vol. 53, no. 1, pp. e12217, 2017.

[21] B. Koohbor, S. Ravindran and A. Kidane, "Experimental Determination of Representative Volume Element (RVE) Size in Woven Composites," *Optics and Lasers in Engineering,* vol. 90, pp. 59-71, 2016.

[22] J. Stinville, W. Lenthe, M. Echlin, P. Callahan and D. Texier, "Microstructural statistics for fatigue crack initiation in polycrystalline nickel-base superalloys," *International Journal of Fracture,* vol. 208, pp. 221-240, 2017.

[23] M. Sutton, W. Wolters, W. Peters, W. Ranson and S. McNeill, "Determination of displacements using an improved digital correlation method," *Image and vision computing,* vol. 1, no. 3, pp. 133-139, 1983.

[24] J. Carroll, W. Abuzaid, J. Lambros and H. Sehitoglu, "An experimental methodology to relate local strain to microstructural texture," *Review of Scientific Instruments,* vol. 81, no. 8, 2010.

[25] J. Schindelin, I. Arganda-Carreras, E. Frise, V. Kaynig, M. Longair, T. Pietzsc, S. Preibisch, C. Rueden, S. Saalfeld, B. Schmid, J. Tinevez, D. White, V. Hartenstein, K. Eliceiri, P. Tomancak and A. Cardona, "Fiji: an open-source platform for biological image analysis," *Nature Methods,* vol. 9, no. 7, pp. 676-682, 2012.

[26] R. B. Vieira, H. Sehitoglu and J. Lambros, "Representative Volume Elements for Plasticity and Creep Measured from High-Resolution Microscale Strain Fields," *Submitted to Acta Materialia,* 2021.

[27] R. B. Vieira, “Strain Inhomogeneities During Plasticity and Creep of Metals: Representative Volume Elements and Microscale Strain Predictions”, Doctoral dissertation, University of Illinois at Urbana-Champaign, Urbana, 2021.

[28] B. Mandelbrot and J. van Ness, "Fractional Brownian motions, fractional noises and applications," *SIAM Review,* vol. 10, no. 4, pp. 422-437, 1968.

[29] M. Matsumoto and T. Nishimura. “Mersenne Twister: A 623-Dimensionally Equidistributed Uniform Pseudorandom Number Generator,” ACM Transactions on Modeling and Computer Simulation, vol. 8 no. 1, pp. 3–30, 1998.